Macromolecules

Article

pubs.acs.org/Macromolecules

Direct Visualization of Three-Dimensional Morphology in Hierarchically Self-Assembled Mixed Poly(*tert*-butyl acrylate)/Polystyrene Brush-Grafted Silica Nanoparticles

Saide Tang,[†,⊥] Ting-Ya Lo,[‡,⊥] Jonathan M. Horton,[§] Chunhui Bao,[§] Ping Tang,[∥] Feng Qiu,[∥] Rong-Ming Ho,*[,‡] Bin Zhao,*[,§] and Lei Zhu*[,†]

[†]Department of Macromolecular Science and Engineering, Case Western Reserve University, Cleveland, Ohio 44106-7202, United States

[‡]Department of Chemical Engineering, National Tsing Hua University, Hsinchu 30013, Taiwan

[§]Department of Chemistry, University of Tennessee, Knoxville, Tennessee 37996, United States

[∥]Department of Macromolecular Science, Fudan University, Shanghai 200433, P. R. China

Supporting Information

ABSTRACT: Three-dimensional (3D) morphology of hierarchically self-assembled mixed poly(*tert*-butyl acrylate) (P*t*BA)/polystyrene (PS) brush-grafted 67 nm silica nanoparticles cast from chloroform on a carbon-coated transmission electron microscopy (TEM) grid was directly visualized using electron tomography (i.e., 3D TEM). The number-average molecular weights for P*t*BA and PS were 22.2 and 23.4 kDa, and their grafting densities were 0.51 and 0.34 chains/nm^2, respectively. For a dense monolayer of mixed brush-grafted silica particles, a rippled phase structure was observed, and the monolayer consisted of protruded top portions from large nanoparticles and a bottom continuous film. In the top protruded part of large nanoparticles, isolated cylindrical PS microdomains were formed in the P*t*BA matrix due to the low PS volume fraction (i.e., 37%). The morphology in the lower continuous film was strongly influenced by interparticle interactions via mixed polymer brushes. As a result, bicontinuous nanostructures instead of isolated PS microdomains in the P*t*BA matrix were formed, even though the PS was a minor phase. In the continuous film, the top and bottom regions gave better microphase separation due to the larger interstitial spaces, and the microphase-separated pattern was dictated by the hexagonal packing of hairy silica particles. For isolated individual particles cast from chloroform, different morphology was observed because of the lack of interparticle interactions. Clear lateral microphase separation was observed only in the bottom part of the particle, likely because the mixed brush layer in the top portion was too thin. In the bottom part, isolated PS microdomains with a truncated wedge shape radiated out from the projected center of the individual particle. This is the first time that detailed 3D morphology was thoroughly characterized for self-assembled mixed brush-grafted nanoparticles cast from a nonselective good solvent.

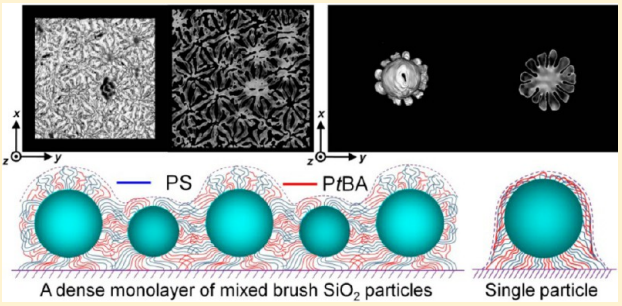

INTRODUCTION

Representing a novel class of environmentally responsive materials, mixed homopolymer brushes grafted on either flat or curved (e.g., nanoparticles or nanorods) substrates have attracted substantial attention for both fundamental and practical research.[1,2] For immiscible binary mixed brushes, two chemically distinct homopolymers are randomly or alternately grafted by one end on the substrate, and nanophase separation is driven by their incompatibility to minimize the system's overall free energy. For symmetric binary mixed brushes (i.e., both homopolymers have the same chain length and grafting density) on a flat substrate, different types of microphase separation are possible, namely, lateral or vertical phase separation, or combination of the two. For lateral phase separation, two immiscible polymers (A and B) have to pass around each other, forming a finite mixing layer next to the substrate, in order to segregate into a rippled structure in the top layer. The domain size is predicted to be on the order of the root-mean-square end-to-end distances ($\langle R_{rms} \rangle$) of respective polymers.[3,4] For vertical phase separation, one polymer, e.g., A polymer, is strongly stretched away from the substrate, forming a separate top layer protecting the bottom layer comprised of individually stretched A polymer chains and collapsed B polymer chains. The third scenario is the combined lateral/vertical phase separation, in which two polymers in the bottom layer undergo distinctive lateral phase separation and

Received: June 18, 2013
Revised: July 29, 2013
Published: August 9, 2013

 © 2013 American Chemical Society dx.doi.org/10.1021/ma401264m | *Macromolecules* 2013, 46, 6575−6584

one polymer is further stretched out to form a surface layer due to a favorable interaction with the environment (e.g., air or solvent).

Early theoretical studies indicated that lateral rather than vertical phase separation with a rippled structure was preferred for symmetric binary mixed brushes grafted on a flat substrate under either equilibrium melt or nonselective solvent conditions.[3−8] This is primarily attributed to the unfavorable interactions of individually stretched A polymer chains with the surrounding B chains in the bottom layer in the vertical phase separation. In the case of favorable interactions between A polymer and the environment, combined lateral/vertical phase separation is preferred, where unfavorable interactions between highly stretched individual A chains and the B matrix in the bottom layer can be avoided by microphase separation. If B polymer forms isolated domains in the phase-separated bottom layer, a dimple structure is obtained.[6]

For binary mixed homopolymer brushes grafted on curved substrates, such as micro- or nanoparticles, three scenarios again can be envisioned. First, when the substrate curvature is relatively low (e.g., the particle size larger than 150 nm),[1] the microphase separation between two polymers is hardly affected by the substrate curvature, and thus the situation is similar to the case of flat substrates mentioned above. Second, when the particle size is similar to the values of the $\langle R_{rms} \rangle$ of grafted polymer chains, many novel nanostructures, e.g., ordered polyhedral or island-like structures, have been predicted for mixed brushes by computer simulation.[9,10] Third, when the substrate curvature is very high (i.e., the size of nanoparticles is much smaller than the $\langle R_{rms} \rangle$ of grafted polymers), the mixed brush-grafted particles behave like miktoarm star copolymers, which can form Janus particles with various self-assembly possibilities.[11−13] In addition to symmetric binary mixed brushes, asymmetric mixed brushes can exhibit a rich variety of microphase-separated morphologies under melt and solvent conditions, which are intimately determined by the relative chain lengths and grafting densities of the two tethered polymers.[6−10] Nonetheless, the fundamental features of lateral and combined lateral/vertical microphase separation are still preserved for asymmetric mixed brushes regardless of flat or curved substrates.

Inspired by theoretical and simulation predictions, experimental investigation of microphase separation for mixed brushes on flat and curved substrates began about a decade ago.[14−19] Both lateral and combined lateral/vertical phase separations, which result in rippled and dimpled nanostructures, respectively, have been observed experimentally. A variety of characterization tools were employed to elucidate the morphology of microphase-separated mixed brushes. For example, atomic force microscopy (AFM) was often used to study the topology of mixed brushes on flat substrates.[20,21] The limitation of conventional AFM lies in the fact that only the surface morphology can be obtained; the internal structure of mixed brushes has to be speculated. To overcome this difficulty, the internal structure of mixed polystyrene (PS)/poly(methyl methacrylate) (PMMA) brushes grafted on a silicon wafer was characterized by combining step-by-step oxygen plasma etching and AFM imaging (i.e., AFM tomography).[22] Nonetheless, three-dimensional (3D) reconstruction of the internal structure using this technique could be difficult because the etching rates for different polymers were different.

Transmission electron microscopy (TEM) is another powerful tool for direct visualization of nanostructures formed by mixed brushes, especially grafted on particles. In a particular effort, we previously used conventional TEM to investigate the microphase-separated morphology of mixed poly(*tert*-butyl acrylate) (P*t*BA)/PS brushes grafted on relatively large silica particles.[23−27] For nearly symmetric mixed P*t*BA/PS brushes grafted on 160−180 nm silica particles, lateral phase separation with bicontinuous worm-like P*t*BA and PS nanodomains was observed under equilibrium melt condition[23] and after being cast from a nonselective good solvent such as chloroform.[24] By varying the PS chain length from shorter than to comparable to, and longer than that of P*t*BA with a constant molecular weight of 24.5 kDa, the morphology of mixed brushes evolved from isolated PS nanodomains in the P*t*BA matrix, to bicontinuous, random worm-like nanostructures, and to a two-layer structure in which the bottom layer was laterally phase-separated and covered by the longer polymer chains.[25,26] In addition, the overall grafting density ($\sigma_{overall}$) played an important role in the microphase separation of mixed P*t*BA/PS brushes.[27] At a low $\sigma_{overall}$ ($\leq$0.20 chains/nm^2), no microphase separation was observed. Upon increasing the $\sigma_{overall}$ to 0.34 chains/nm^2, lateral microphase separation between grafted P*t*BA and PS chains produced rippled nanostructures. The ripple wavelength decreased upon increasing $\sigma_{overall}$ and scaled as $\sigma_{overall}^{-0.47}$ in a range of 0.54−1.06 chains/nm^2.

As mentioned earlier, the substrate curvature plays a very important role in the microphase separation of mixed homopolymer brushes.[9,10] We recently synthesized a series of mixed P*t*BA/PS brushes grafted on 67 nm silica nanoparticles[28] and observed truncated wedge-shaped nanodomains on the basis of conventional bright-field TEM images, which were believed to be the result of the increased substrate curvature (i.e., smaller nanoparticle size). However, limited by the two-dimensional (2D) projection images in conventional TEM, the information on the 3D self-assembly of mixed brushes grafted on nanoparticles cannot be obtained. Recently, electron tomography (or 3D TEM) has advanced substantially and is often used to investigate polymer nanostructures. By taking advantage of 3D visualization in high resolution and effective real-space reconstruction, the microphase-separated structures of a variety of polymers have been visualized.[29−34]

In this work, we used electron tomography to reconstruct hierarchical self-assembly of mixed P*t*BA/PS brush-grafted 67 nm silica nanoparticles cast from a nonselective good solvent, chloroform. The size distribution of silica nanoparticles was relatively broad, in the range of 50−90 nm. It was found that both particle size distribution and interparticle interactions through grafted mixed brushes dictated the 3D self-assembly of mixed P*t*BA/PS brushes in a dense monolayer of hairy silica nanoparticles. For individual particles, different morphology was observed primarily owing to the lack of interparticle interactions.

EXPERIMENTAL SECTION

Materials. Snowtex-ST-OL (silica nanoparticles with a size of 40−50 nm, according to the manufacturer, in a 20 wt % aqueous dispersion) was provided by Nissan Chemical USA. Our TEM result showed that after centrifugation the particle size ranged from ~50 to ~90 nm with an average size of 67 nm. Mixed poly(*tert*-butyl acrylate) (P*t*BA)/polystyrene (PS) brushes were synthesized by sequential atom transfer radical polymerization (ATRP) of *t*BA and nitroxide-mediated radical polymerization (NMRP) of styrene from Y-initiator-functionalized silica nanoparticles. The experimental details can be found in our previous publication.[28] The number-average molecular weight (M_n) and the polydispersity index (PDI) of P*t*BA were 22.2 kDa and

1.19, respectively. The M_n and the PDI of PS were 23.4 kDa and 1.17, respectively. The grafting densities of P*t*BA and PS were 0.54 and 0.31 chains/nm^2, respectively.

Characterization Methods and Instrumentation. For the electron tomography (3D TEM) study, mixed P*t*BA/PS brush-grafted silica nanoparticles were dispersed in chloroform, a nonselective good solvent for both P*t*BA and PS. The sample was drop-cast onto a carbon-coated TEM grid and dried at ambient temperature. The sample was then annealed with $CHCl_3$ vapor in a closed container for 3 h, followed by staining with RuO_4 vapor at room temperature for approximately 20 min. On the basis of our previous work,[25,26] there was no significant difference between thermal (120 °C for 3 h) and solvent (chloroform vapor at room temperature for 3 h) annealing processes. Meanwhile, no obvious difference in microphase separation was observed after the sample was annealed in $CHCl_3$ vapor beyond 1 h. Electron tomography of the mixed brush-grafted silica nanoparticles was carried out using a JEOL (JEM-2100) TEM operated at 200 kV. The as-cast sample on the TEM grid was further carbon coated to reduce the charging problem due to long-time exposure under electron beam for collection of projection images from different tilting conditions. A series of 71 TEM projection images were collected from −70° to +70° tilt angles at an angular interval of 2°. Images were recorded on a Gatan CCD camera. Alignment of the tilt series and corresponding 3D reconstruction were performed using IMOD software with fiducialless alignment. The reconstructed volume was then filtered by a 5 × 5 × 5 median filter for noise reduction. The contrast of filtered images was further enhanced with high dynamic range (HDR) toning by Photoshop CS5 software. 3D analyses such as binarization, segmentation, and visualization of the volume of interest were performed using the Analyze 4.0 software. To further investigate the internal structure of mixed P*t*BA/PS brushes, a series of *z*-scan and *x*-scan images were retrieving by digitally slicing the 3D reconstructed box with different *z* and *x* positions. The *z* direction was normal to the substrate, and the *x* direction was the longitudinal direction in the 2D TEM image. A new method to extract a single particle from a 3D box was carried out by trimming all the image frames with a circular mask. By using the digital slice image from different directions, the internal structure of complicated reconstructed image in real space can be successfully visualized, giving detailed textures of the mixed brush-grafted nanoparticles and offering a new methodology for electron tomography analysis.

For the X-ray photoelectron spectroscopy (XPS) study, PS (21 kDa and PDI = 1.04), P*t*BA (23 kDa and PDI = 1.15 from Polymer Source, Inc.), and mixed P*t*BA/PS brush-grafted silica nanoparticles were dissolved/dispersed in chloroform and drop-cast onto clean silicon wafers. The cast samples were annealed with $CHCl_3$ vapor in a closed container for 3 h. XPS spectra were recorded on a PHI VersaProbe 5000 scanning ESCA microprobe using a monochromated X-ray beam (Al anode) with a 300 μm diameter/65 W X-ray beam at takeoff angles of 30°, 45°, and 90°. XPS survey scans were taken at a pass energy of 93.9 eV, and high-resolution scans were taken at a pass energy of 23.5 eV in regions of Si 2p, C 1s, and O 1s. Data analysis was conducted using the Multipak software (Physical Electronics, Inc., Chanhassen, MN).

RESULTS AND DISCUSSION

3D Morphology in a Dense Monolayer of Mixed P*t*BA/PS Brush-Grafted Silica Nanoparticles. Figure 1A shows a typical bright-field, conventional TEM micrograph of mixed P*t*BA/PS brush-grafted 67 nm silica nanoparticles. The sample was stained by RuO_4 vapor at room temperature for 20 min. Similar TEM images were reported in a recent letter.[28] Note that RuO_4 selectively stained PS;[35] therefore, the phase-separated PS and P*t*BA nanodomains appeared dark and bright, respectively. The silica cores, ranging from 50 to 90 nm, could be identified with a gray contrast, due to an appropriate degree of staining of the sample. The hairy nanoparticles packed closely into a hexagonal array, which was also observed

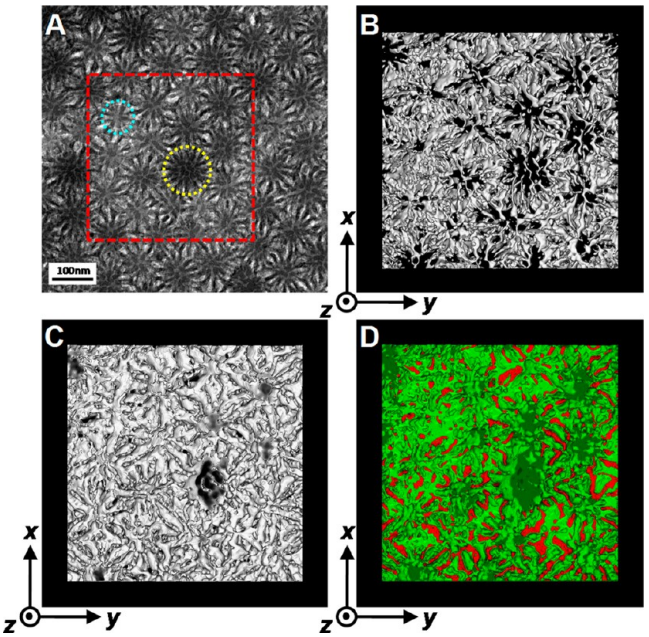

Figure 1. (A) Bright-field TEM micrograph of a dense monolayer film of mixed P*t*BA/PS brush-grafted 67 nm silica nanoparticles stained by RuO_4 vapor for 20 min. The red box indicates the area for reconstructed 3D image. The yellow and blue dotted circles highlight a large (90 nm) and a small (53 nm) nanoparticle, respectively. (B) Top-view 3D TEM image of the reconstructed box with visible P*t*BA and PS/SiO_2 are invisible. (C) Top-view 3D TEM image of the reconstructed box with visible PS/SiO_2 and P*t*BA is invisible. (D) Top surface image with combined P*t*BA (red) and PS (green) after 3D reconstruction.

for other hairy particles on a flat substrate.[24−26] This could be caused by the bridging effect of grafted polymer brushes across the interstitial space among silica particles. The mixed P*t*BA/PS brushes grafted on the medium and small silica nanoparticles showed a nearly bicontinuous, worm-like pattern, which was the typical microphase separation morphology for symmetric mixed brushes.[24−26] For large particles, a few isolated dark PS domains, ca. 12.5 nm in diameter, appeared in the center of the particle (e.g., indicated by the yellow circle in Figure 1A). On the basis of this observation,[28] we concluded that mixed P*t*BA/PS brushes were laterally phase separated, and the PS domains appeared as truncated wedge-shaped nanostructures, which were attributed to the curvature effect from 67 nm silica nanoparticles. It should be emphasized here that the micrograph in Figure 1A is a 2D projection image; the internal 3D nanostructure of microphase separated mixed brushes was unknown and had never been presented before.

To identify the 3D microphase-separated structure, electron tomography was utilized to visualize the self-assembly in a close-packed monolayer film of mixed brush-grafted silica nanoparticles on a carbon-coated TEM grid. Here, a 480 × 480 nm^2 area (see the red box in Figure 1A) was selected for 3D reconstruction from electron tomography using the Analyze 4.0 software. Figures 1B and 1C show the top views of this reconstructed 3D box with exclusive P*t*BA and PS/SiO_2 phases, respectively. The corresponding 3D movies for both P*t*BA and PS phases are shown in Movies S1 and S2 in the Supporting Information. From Figures 1B and 1C and the movies, both P*t*BA and PS phases exhibited a worm-like bicontinuous

dx.doi.org/10.1021/ma401264m | *Macromolecules* 2013, 46, 6575−6584

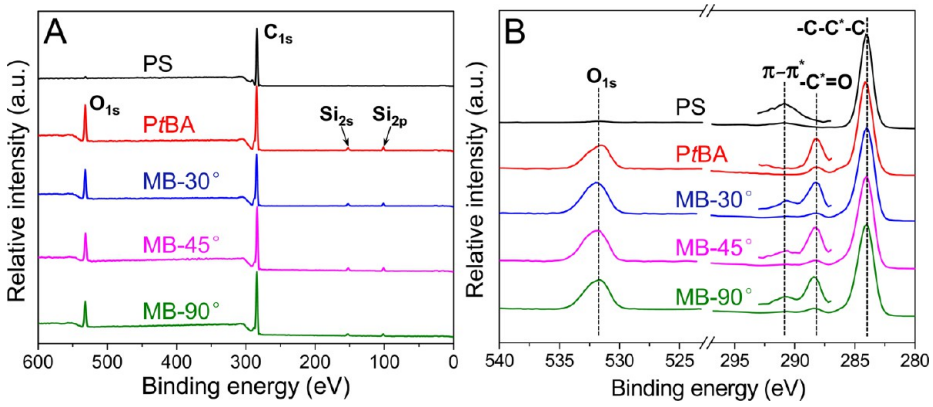

Figure 2. (A) XPS survey scans for PS and P*t*BA homopolymers (90° takeoff angle) and P*t*BA/PS mixed brush (MB, grafted on 67 nm silica particles) film tested at takeoff angles of 30°, 45°, and 90°, respectively. (B) High-resolution XPS scans for the C_{1s} and O_{1s} regions for PS and P*t*BA homopolymers (90° takeoff angle) and mixed P*t*BA/PS brushes (MB) film tested at takeoff angles of 30°, 45°, and 90°, respectively. The spectra in the 293−287 eV region are magnified as insets.

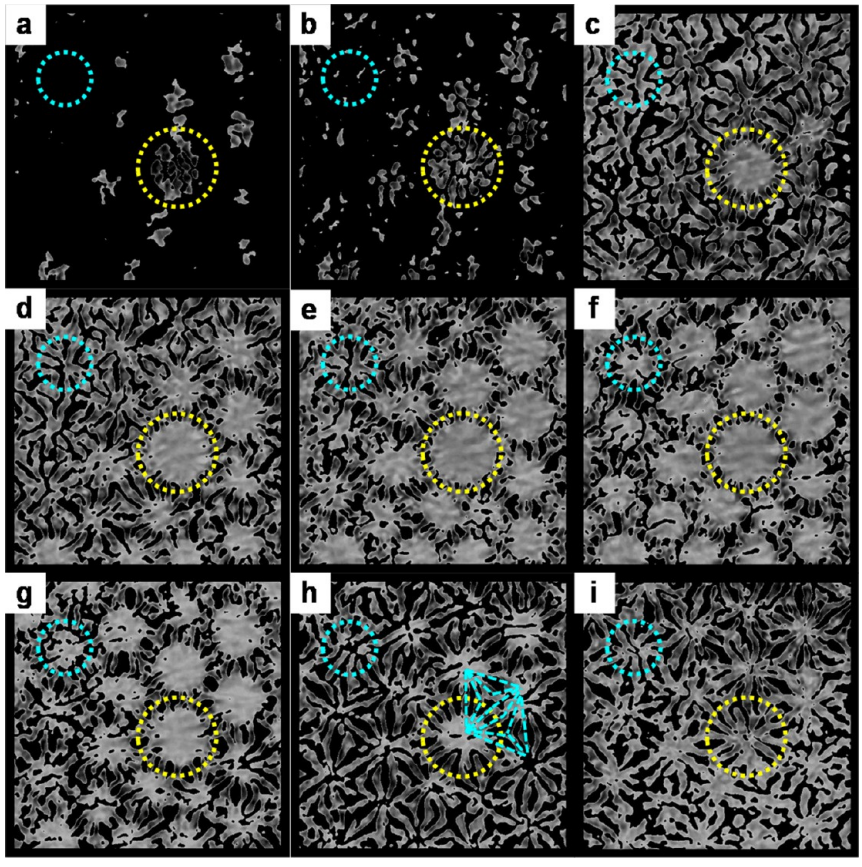

Figure 3. (a−i) Consecutive *z*-scan TEM images of the 3D reconstructed box in Figure 1C. Each image is located at a 12 nm interval. The yellow and blue dotted circles indicate positions of the large (90 nm) and small (53 nm) particles, respectively. The blue dashed lines in (h) represent the 3-fold connections of PS microdomains among neighboring particles.

nanostructure with microdomains connecting in three dimensions.

First of all, we were interested in the microphase separation at the very top surface (i.e., the brush−air interface) of the mixed P*t*BA/PS brushes. Figure 1D shows the top-view (or surface) image of the 3D reconstructed box with P*t*BA (red) and PS (green) nanodomains combined together. It was seen that both P*t*BA and PS were present in the very top surface of the film. This was consistent with the rippled nanostructure of mixed P*t*BA/PS brushes having similar molecular weights. However, the fraction of the P*t*BA phase appeared to be less than that of the PS phase. Considering the P*t*BA volume fraction of 63% in the brush layer,[36] this seemed unreasonable. Several reasons might be possible for this observation. First, the chain length of P*t*BA (DP = 172) was slightly shorter than PS (DP = 225), although its volume fraction was higher. Second, the P*t*BA phase at the top surface was likely underestimated due to the difficulty in differentiating the unstainable P*t*BA from the vacuum in the 3D reconstruction. We believe that the latter

dx.doi.org/10.1021/ma401264m | *Macromolecules* 2013, 46, 6575−6584

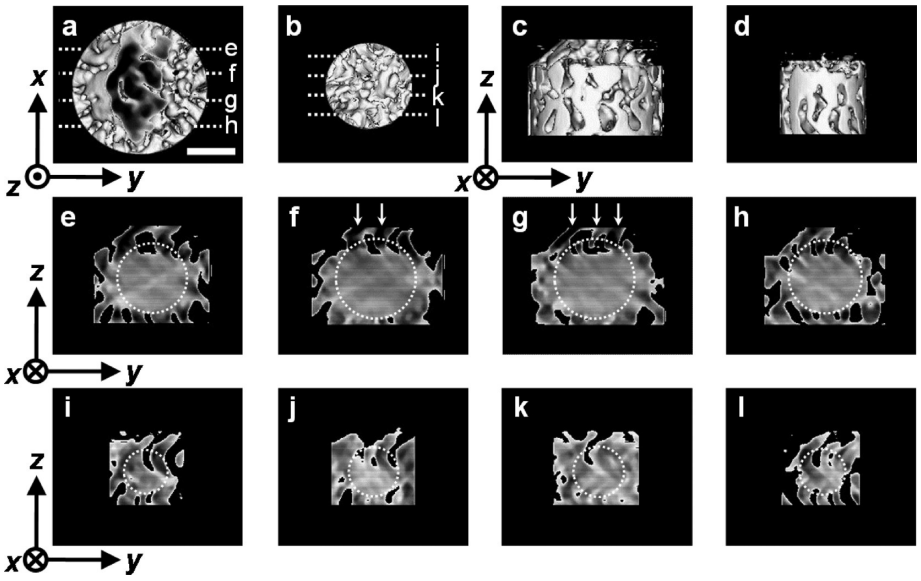

Figure 4. (a, b) Top-view and (c, d) side-view reconstructed TEM images of the morphology from a large (90 nm) and a small (53 nm) particle. (e–h) *x*-scan images of the morphology from the large particle and the positions are indicated in (a). (i–l) *x*-scan images of the morphology from the small particle and the positions are indicated in (b). White dotted circles show possible cross sections of the silica cores. All images share the same scale bar of 50 nm, as shown in (a).

is the major reason for the low P*t*BA content in the top view image in Figure 1D.

The coexistence of P*t*BA and PS at the very top surface of the mixed brush film seemed inconsistent with a recent report that P*t*BA had a lower surface energy (31.2 mN/m) than PS (40.7 mN/m) and tended to segregate to the film–air interface in PS-*b*-P*t*BA block copolymer thin films spun-coated on a silicon wafer substrate.[37] We considered that the situation for the mixed P*t*BA/PS brushes here was different because both P*t*BA and PS chains were end-tethered to the silica nanoparticles. To confirm the coexistence of both P*t*BA and PS in the very top layer of the mixed brush film, XPS was carried out for mixed P*t*BA/PS brush-grafted silica particles at different takeoff angles. In the survey scan spectra (Figure 2A), both C_{1s} and O_{1s} peaks were seen for the P*t*BA/PS mixed brush film at different takeoff angles, while weak Si_{2s} and Si_{2p} peaks, from silica nanoparticles and/or the silicon wafer substrate, were also observed. For high-resolution spectra in the C_{1s} and O_{1s} regions (Figure 2B), C_{1s} peaks (from the backbone $-CH_2CH-$ carbon atoms) were assigned to a binding energy of 284.0 eV in order to correct for the charging energy shift. For both P*t*BA homopolymer and mixed P*t*BA/PS brushes, the O_{1s} peaks at 531.8 eV were clearly seen, while no O_{1s} peak appeared for the PS homopolymer. In the C_{1s} region, the sharp peak at 284.0 eV, assigned to the carbon atoms in the polymer backbone, was observed for all samples. The carbonyl C_{1s} peaks at 288.2 eV were present in the spectra of P*t*BA and mixed P*t*BA/PS brush films. The broad peak at 290.8 eV, which was assigned to the shakeup peak associated with the $\pi-\pi^*$ transition of the benzene ring, was observed in the spectra of PS and the mixed P*t*BA/PS brush films. The coexisting peaks from P*t*BA and PS in the XPS spectra for the mixed P*t*BA/PS brush film at different takeoff angles confirmed that both P*t*BA and PS were present at the top surface layer of the self-assembled hairy particle film. In addition, the XPS spectra for the mixed P*t*BA/PS brush film at different takeoff angles were almost the same, revealing a similar composition in the mixed brush film within the top 5–10 nm depth. Note that quantitative analysis of the P*t*BA/PS ratio was not possible, primarily due to the degradation of the P*t*BA upon X-ray beam irradiation.

To investigate the internal structure of mixed P*t*BA/PS brushes, *z*-scan images from the 3D reconstructed box in Figure 1C are presented in Figure 3. From the top (Figure 3a) to the bottom layer (Figure 3i) with an interval of 12 nm, the morphology of PS and SiO_2 phases was clearly seen. At the very top layer (Figures 3a,b), a few isolated PS domains were seen on the protruded portion of large silica particles (e.g., see inside of the yellow circle). Comparing with the 2D TEM image in Figure 1A, these isolated PS domains in Figures 3a,b matched well with the isolated dark domains located in the center of the large particle (indicated by the dotted yellow circle) in Figure 1A. This could be attributed to the fact that the PS volume fraction was 37 vol % in the mixed brushes.

Below the protruded portions of large particles, Figures 3c,d show the *z*-scan images at the top region of the continuous dense film. At these levels, the silica cores of large particles were seen. Both (bright) PS and (dark) P*t*BA domains radiated outward from the center of the silica core and connected with the corresponding domains from neighboring particles. Different from the protruded top layer morphology, the PS and P*t*BA phases formed a bicontinuous radiating morphology in most areas, regardless of the PS volume fraction being only 37%. For small particles (e.g., see the blue circle), no isolated PS domains were seen, and the morphology was directly transformed to bicontinuous phase separation. This could be attributed to the strong interparticle interactions through mixed polymer brushes.

In the middle region of the continuous dense film (Figures 3e–g), the silica core of each particle could be clearly identified. The phase-separated P*t*BA and PS domains could still be seen in the interstitials of silica nanoparticles. Compared to the phase separation in the upper region of the continuous film (Figures 3c,d), the phase separation of mixed P*t*BA and PS brushes in the middle region (Figures 3e–g) appeared to be less organized. This could be attributed to the limited interstitial space among the silica cores in the middle region.

dx.doi.org/10.1021/ma401264m | *Macromolecules* 2013, 46, 6575–6584

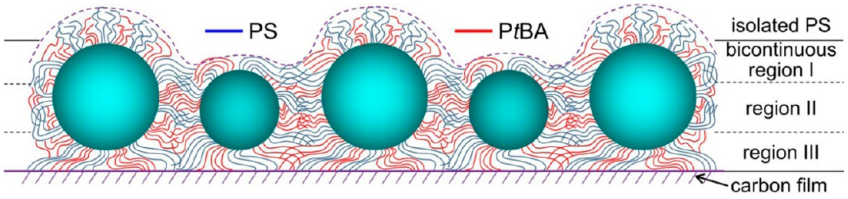

Figure 5. Schematic illustration of a dense monolayer of mixed P*t*BA/PS brush-grafted silica nanoparticles. The P*t*BA and PS chains are in red and blue, respectively. Silica particles are in cyan color.

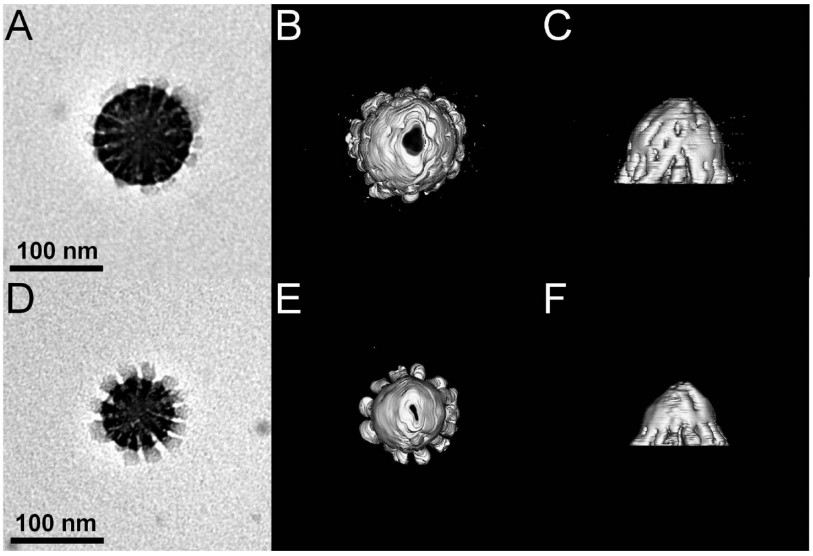

Figure 6. (A, D) Bright-field 2D TEM images and (B, E) top-view and (C, D) side-view reconstructed 3D TEM images of a large (~80 nm) and a small (~50 nm) particle, respectively.

Figures 3h,i show the *z*-scan images for the bottom region of the continuous film. Different from the top and middle regions of the continuous film, the bottom region showed the best phase separation morphology due to the large space between silica nanoparticles and the carbon film substrate. Again, both PS and P*t*BA microdomains radiated out from the projected center of the silica core, producing bridges among neighboring nanoparticles. Quite a few PS bridges (especially for small nanoparticles) showed a truncated wedge shape at both ends. This is consistent with the observation in our previous report.[28] Judging from the bright-field TEM micrograph in Figure 1A, conventional 2D TEM images must have focused on the bottom region of the continuous film in order to achieve the best image for microphase separation. In Figure 3h, the pattern of microphase separation was dictated by the hexagonal packing of silica nanoparticles. An example was shown among four close-packed nanoparticles connected by blue dashed lines, and the pattern consisted of two triangles with 3-fold symmetry.

To further examine the internal 3D structures, we dug out a large (90 nm) and a small (53 nm) particle from Figure 1C, and their top and side views are shown in Figures 4a–d. Note that these particles correspond to those highlighted with dotted yellow and blue circles in Figure 1A. From the side views in Figures 4c,d, it was clear that both PS and P*t*BA formed bicontinuous separated phases even along the *z* direction. Judging from the images in Figures 4c,d, the protruded part was about 30% of the total height of the large particle. From the *x*-scan images of the large particle (Figures 4e–h), isolated PS domains stretched upward from the upper portion of the silica core (see the arrows; note that the inside of the vertical PS domains did not appear very bright possibly due to certain artifact from 3D reconstruction). Combining with the *z*-scan image in Figure 3b, we concluded that isolated PS domains in the protruded top layer should have a short cylindrical shape, and this was consistent with the PS volume fraction of only 37%. Note that isolated PS domains only existed in the protruded top part of the large particle, and they did not form any bicontinuous structure because the protruded part was isolated and there were no interparticle interactions. From Figures 4e–h, we noticed that the cross sections of the large particle did not show a circular shape (see the dotted circles for the supposed cross section of the silica core). We speculate that this particle might have an ellipsoidal shape. From the *x*-scan images of the small particle (Figures 4i–l), no isolated PS domains stretched out from the top of the silica core. Instead, P*t*BA and PS domains were bicontinuous. This was consistent with bicontinuous worm-like phase separation observed in the above *z*-scan images (Figure 3c) and conventional 2D TEM image (Figure 1A). We noticed that some voids existed inside the supposed cross sections of the silica cores (i.e., the white dotted circles) in the *x*-scan images, especially for the small particle. This might be attributed to certain artifacts from data treatment during 3D reconstruction of the TEM images.

On the basis of the above 3D TEM results, a layered nanostructure existed in a dense monolayer of mixed P*t*BA/PS brush-grafted silica nanoparticles, primarily owing to the polydispersity in particle size (ca. 50–90 nm) and strong interparticle interactions, as illustrated in Figure 5. In the top ripple layer (i.e., the protruded parts of large particles), PS chains formed isolated short cylindrical domains in the P*t*BA

dx.doi.org/10.1021/ma401264m | *Macromolecules* 2013, 46, 6575–6584

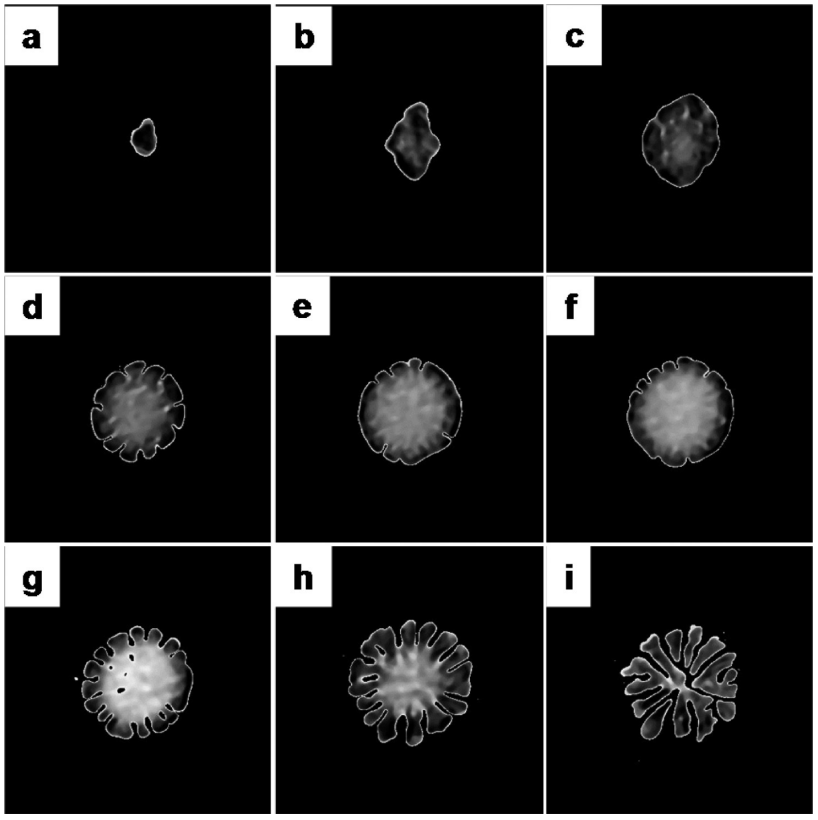

Figure 7. (a–i) Consecutive *z*-scan TEM images of the reconstructed large particle (~80 nm) in Figure 6B. Each image is located at a ca. 11 nm interval.

matrix. This is because the protruded parts of large particles were more or less isolated, and PS was a minor component with a volume fraction of 37%. In the continuous film, P*t*BA and PS chains formed a bicontinuous structure because of strong interparticle interactions via mixed brushes. In this continuous film, the top and bottom portions had better phase-separated PS and P*t*BA microdomains, and this was attributed to the large interstitial spaces among particles. In particular, the bottom region, which was in contact with the carbon film, had the best microphase separation. The hexagonal packing of silica nanoparticles dictated the pattern of microphase-separated mixed P*t*BA/PS brushes. For example, truncated wedge-shaped PS and P*t*BA domains formed a radiating structure from the projected centers and interconnected between neighboring nanoparticles, conforming to the 3-fold symmetry. In the middle region of the continuous film, microphase separation was poor due to the limited interstitial space among silica nanoparticles.

3D Morphology in Single Mixed P*t*BA/PS Brush-Grafted Silica Nanoparticles. From the above results, the interparticle interactions via mixed brushes are important for the morphology formation in a dense monolayer of mixed brush-grafted silica nanoparticles cast from chloroform. A question naturally stands out: what will the 3D morphology be for individual mixed brush-grafted particles without any interparticle interaction? On the same TEM grid, individual nanoparticles were also observed, and electron tomography was employed to obtain their 3D morphology. Figures 6A and 6D show bright-field conventional TEM images for a large and a small mixed brush-grafted silica nanoparticle, respectively. Comparing with the dense monolayer (Figure 1A), the silica cores were only weakly discernible, and it seemed that these individual particles were slightly overstained by RuO_4. Since both the dense film and individual particles were on the same TEM grid, we consider that the dense film effectively reduced the diffusion of RuO_4 vapor into the bottom of the film, while individual particles did not. From these bright-field TEM images, we roughly obtained the silica core sizes to be ~80 and ~50 nm for the large and small particles, respectively, and they were comparable to those large and small particles in the dense film in Figure 1A. For the large particle (Figure 6A), no isolated PS domains were observed in the center, as seen for the large particle in Figure 1A. Instead, truncated wedge-shaped PS domains radiated outward from the center. At the periphery, these PS wedges even extended beyond the dark contour of the hairy nanoparticle. For the small particle (Figure 6D), similar morphology was observed but with more obvious truncated PS wedges radiating outward from the center. This is consistent with our recent report and is considered to be caused by the curvature effect of small silica nanoparticles.[28]

3D morphology for both large and small hairy particles is shown in Figures 6B,C (top views) and 6E,F (side views), respectively, with visible PS/SiO_2 phases. From the side views (Figures 6C,F), bell-shaped instead of spherical particles were observed. We consider that this should result from the solution-casting procedure. As chloroform evaporated, mixed P*t*BA/PS brushes were pulled down toward the carbon substrate by the evaporating meniscus. This eventually resulted in less polymer on the top than at the bottom of the particles, forming an overall bell shape. The pulled-down mixed brushes formed a skirt of film covering the bottom carbon surface with clear microphase separation between P*t*BA and PS, whereas the

dx.doi.org/10.1021/ma401264m | *Macromolecules* 2013, 46, 6575–6584

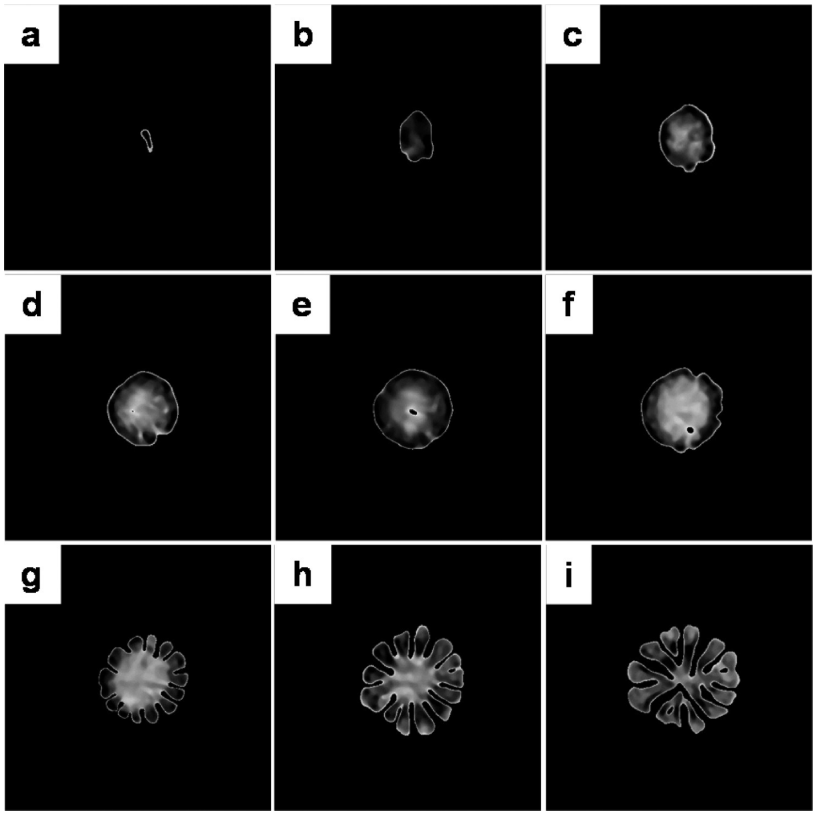

Figure 8. (a–i) Consecutive *z*-scan TEM images of the reconstructed small particle (~50 nm) in Figure 6E. Each image is located at a ca. 8 nm interval.

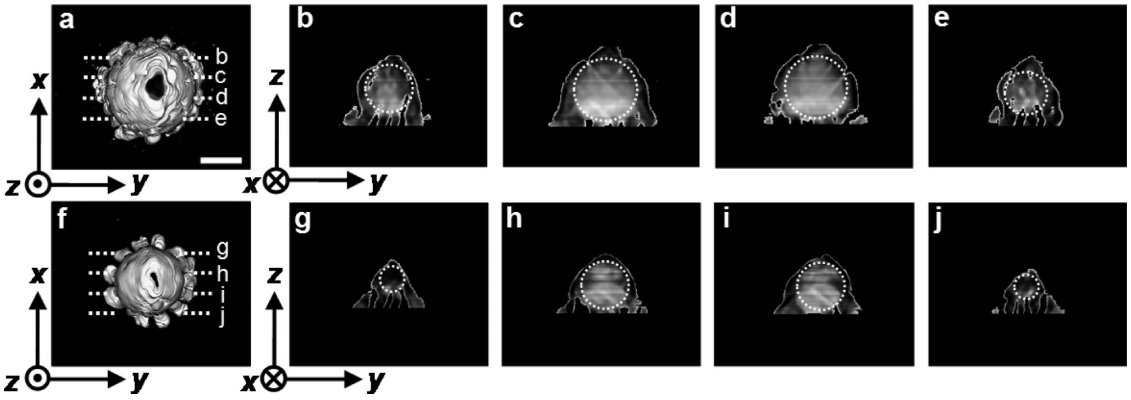

Figure 9. (a, f) Top-view 3D TEM images of a large (~80 nm) and a small (~50 nm) particle, respectively. (b–e) *x*-scan images of the morphology from the large particle and the positions are indicated in (a). (g–j) *x*-scan images of the morphology from the small particle and the positions are indicated in (f). White dotted circles show possible cross sections of the corresponding silica cores. All images share the same scale bar of 50 nm, as shown in (a).

microphase separation in the top portion of the particles was not obvious.

To obtain the internal 3D morphology, *z*-scan images for the large and small nanoparticles are shown in Figures 7 and 8, respectively. No obvious microphase separation between P*t*BA and PS was observed for the top portion of both hairy particles (see parts a–c in Figures 7 and 8). This is drastically different from the hairy particles in the dense monolayer film (see Figure 3). At the bottom parts of both particles, obvious microphase separation was observed (see parts g–i in Figures 7 and 8). Both PS and P*t*BA microdomains showed truncated wedge shapes, radiating outward from the projected centers of the nanoparticles. In the middle portions, the large particle seemed to show weak phase separation (see parts d–f in Figure 7), and this was different from the small particle (see parts d–f in Figure 8). Comparing these *z*-scan results with the bright-field images in Figures 6A,C, conventional TEM again was focused on the bottom portions of these individual particles in order to obtain the best quality images. Note that the bicontinuous morphology in the dense monolayer film was not observed because no interparticle interactions existed for individual particles. Considering the volume fraction of PS brushes of 37%, truncated wedge-like PS microdomains at the bottom should be surrounded by P*t*BA.

The *x*-scan images for both large and small single particles are shown in Figure 9. From these images, it was confirmed

dx.doi.org/10.1021/ma401264m | *Macromolecules* 2013, 46, 6575–6584

that well-defined microphase separation of mixed P*t*BA/PS brushes were seen in the bottom portions, rather than in the top regions of individual particles. White dotted circles showed supposed cross sections of the silica cores at each scan position. It was seen that the mixed brush layer in the top portions of individual particles were too thin (~5−10 nm) to induce microphase separation of mixed P*t*BA and PS brushes. We could attribute this to the solution-casting process, which spread the brush layer to a thin layer.

From the above 3D TEM results, a schematic representation of solution-cast individual particles on a carbon substrate is shown in Figure 10. In the top hemisphere of a single particle,

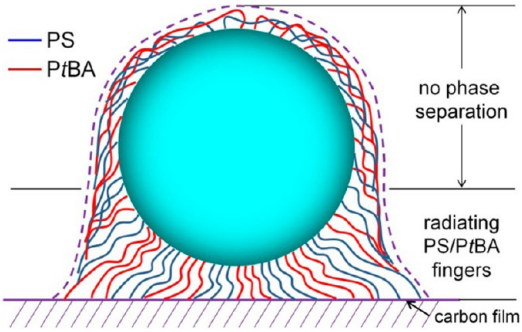

Figure 10. Schematic illustration of an individual, mixed P*t*BA/PS brush-grafted silica nanoparticle. The P*t*BA and PS chains are in red and blue, respectively. Silica particles are in cyan color.

the mixed P*t*BA/PS brushes are pulled down toward the carbon film due to the solvent casting process. As a result, the mixed brush layer in the top hemisphere was too thin to induce microphase separation between highly stretched P*t*BA and PS chains. In the bottom hemisphere, the space between the particle and carbon substrate is large enough for microphase separation. Both PS and P*t*BA microdomains radiate out from the projected center of the silica core.

There are several levels of interactions (of the van der Waals nature) in solution-cast mixed brush-grafted silica particles. First, the interparticle interaction is composed of core−core and brush−brush interactions. The brush−brush interaction should be more important than the core−core interaction in the formation of hexagonal packing scheme, which in turn dictates the microphase separation of mixed brushes at a smaller length scale. Second, during the solution casting process, the solvent−brush interaction strongly influences the conformation and orientation of mixed brushes. As a result, mixed polymer brushes are significantly stretched due to solvent swelling and subsequent evaporation. For instance, the mixed brushes on the top of a single particle are pulled down toward the carbon film substrate during the solvent-drying process, resulting in weak or no microphase separation on the top portion. Third, the brush−substrate interactions include brush−air and brush−carbon substrate interactions. Although there is certain difference between P*t*BA/air and PS/air, no layered structure is formed because the nearly symmetric P*t*BA and PS chains are end-tethered on silica particles. For the brush−carbon film interaction, no quantitative data are currently available for P*t*BA/C and PS/C. On the basis of our experimental results, the carbon film can favorably wet both P*t*BA and PS, and the best microphase separation is observed at the brush−carbon film interface due to the unfavorable interaction between P*t*BA and PS.

CONCLUSIONS

In summary, using electron tomography, we reconstructed 3D nanostructures in hierarchically self-assembled mixed P*t*BA/PS brush-grafted 67 nm silica nanoparticles. For a dense monolayer of the nanoparticles, the microphase-separated structure was intimately dependent upon the polydispersity in particle size distribution and interparticle interactions via the grafted brushes. In the protruded parts of larger particles, PS formed isolated cylindrical domains in the P*t*BA matrix. In the continuous film below the protruded parts, bicontinuous phase separation was caused by strong brush interactions among densely packed silica particles. Larger interstitial spaces at the top and bottom regions of the continuous film resulted in better microphase separation than the middle region. In particular, a clear radiating structure of PS and P*t*BA domains from the projected centers of silica particles was observed in the bottom layer. The radiating structure adopted 3-fold symmetry, which was determined by the hexagonal packing of silica nanoparticles. For individual mixed brush-grafted particles, clear microphase separation was seen in the bottom portion, rather than in the top hemisphere, where the mixed brush layer was as thin as ~5−10 nm. This was considered to be a result of solution casting effect, and mixed brushes were pulled down toward the carbon film during solvent evaporation. In the microphase-separated bottom portion, truncated wedge-shaped domains radiated out from the projected center of the silica particle. This work demonstrates that electron tomography is a powerful characterization tool for understanding the 3D hierarchical self-assembly of mixed brush-grafted inorganic nanoparticles.

ASSOCIATED CONTENT

Supporting Information

Movies for the 3D reconstructed areas in Figures 1B,C, the *z*-scan in Figure 3, Figures 6B,C and 6E,F, and *z*-scans in Figures 7 and 8. This material is available free of charge via the Internet at http://pubs.acs.org.

AUTHOR INFORMATION

Corresponding Author

*E-mail: lxz121@case.edu (L.Z.); rmho@mx.nthu.edu.tw (R.-M.H.); zhao@ion.chem.utk.edu (B.Z.).

Author Contributions

⊥S.T. and T.-Y.L. contributed equally to the work.

Notes

The authors declare no competing financial interest.

ACKNOWLEDGMENTS

This work was supported by the National Science Foundation through Awards DMR-1007918 (L.Z.) and DMR-1007986 (B.Z.). We thank Professor Hiroshi Jinnai of the Kyushu University for the technical exchange of the electron tomography experiments.

REFERENCES

(1) Zhao, B.; Zhu, L. *Macromolecules* **2009**, *42*, 9369−9383.
(2) Stuart, M. A. C.; Huck, W. T. S.; Genzer, J.; Müller, M.; Ober, C.; Stamm, M.; Sukhorukov, G. B.; Szleifer, I.; Tsukruk, V. V.; Urban, M.; Winnik, F.; Zauscher, S.; Luzinov, I.; Minko, S. *Nat. Mater.* **2010**, *9*, 101−113.
(3) Marko, J. F.; Witten, T. A. *Phys. Rev. Lett.* **1991**, *66*, 1541−1544.
(4) Marko, J. F.; Witten, T. A. *Macromolecules* **1992**, *25*, 296−307.

(5) Dong, H. *J. Phys. II* **1993**, *3*, 999−1020.
(6) Müller, M. *Phys. Rev. E* **2002**, *65*, 030802.
(7) Zhulina, E.; Balazs, A. C. *Macromolecules* **1996**, *29*, 2667−2673.
(8) Wang, J.; Müller, M. *J. Phys. Chem. B* **2009**, *113*, 11384−11402.
(9) Roan, J. R. *Phys. Rev. Lett.* **2006**, *96*, 248301.
(10) Wang, Y.; Yang, G.; Tang, P.; Qiu, F.; Yang, Y.; Zhu, L. *J. Chem. Phys.* **2011**, *134*, 134903.
(11) Zubarev, E. R.; Xu, J.; Sayyad, A.; Gibson, J. D. *J. Am. Chem. Soc.* **2006**, *128*, 15098−15099.
(12) Boyer, C.; Whittaker, M. R.; Luzon, M.; Davis, T. P. *Macromolecules* **2009**, *42*, 6917−6926.
(13) Kim, B. J.; Bang, J.; Hawker, C. J.; Chiu, J. J.; Pine, D. J.; Jang, S. G.; Yang, S. M.; Kramer, E. J. *Langmuir* **2007**, *23*, 12693−12703.
(14) Zhao, B.; Brittain, W. J. *Prog. Polym. Sci.* **2000**, *25*, 677−710.
(15) Pyun, J.; Kowalewski, T.; Matyjaszewski, K. *Macromol. Rapid Commun.* **2003**, *24*, 1043−1059.
(16) Edmondson, S.; Osborne, V. L.; Huck, W. T. S. *Chem. Soc. Rev.* **2004**, *33*, 14−22.
(17) Li, D.; Sheng, X.; Zhao, B. *J. Am. Chem. Soc.* **2005**, *127*, 6248−6256.
(18) Barbey, R.; Lavanant, L.; Paripovic, D.; Schuwer, N.; Sugnaux, C.; Tugulu, S.; Klok, H. A. *Chem. Rev.* **2009**, *109*, 5437−5527.
(19) Zdyrko, B.; Luzinov, I. *Macromol. Rapid Commun.* **2011**, *32*, 859−869.
(20) Minko, S.; Muller, M.; Usov, D.; Scholl, A.; Froeck, C.; Stamm, M. *Phys. Rev. Lett.* **2002**, *88*, 035502.
(21) Sui, X.; Zapotoczny, S.; Benetti, E. M.; Schon, P.; Vancso, G. J. *J. Mater. Chem.* **2010**, *20*, 4981−4993.
(22) Usov, D.; Gruzdev, V.; Nitschke, M.; Stamm, M.; Hoy, O.; Luzinov, I.; Tokarev, I.; Minko, S. *Macromolecules* **2007**, *40*, 8774−8783.
(23) Zhao, B.; Zhu, L. *J. Am. Chem. Soc.* **2006**, *128*, 4574−4575.
(24) Zhu, L.; Zhao, B. *J. Phys. Chem. B* **2008**, *112*, 11529−11536.
(25) Jiang, X.; Zhong, G.; Horton, J. M.; Jin, N.; Zhu, L.; Zhao, B. *Macromolecules* **2010**, *43*, 5387−5395.
(26) Jiang, X.; Zhao, B.; Zhong, G.; Jin, N.; Horton, J. M.; Zhu, L.; Hafner, R. S.; Lodge, T. P. *Macromolecules* **2010**, *43*, 8209−8217.
(27) Bao, C.; Tang, S.; Horton, J. M.; Jiang, X.; Tang, P.; Qiu, F.; Zhu, L.; Zhao, B. *Macromolecules* **2012**, *45*, 8027−8036.
(28) Horton, J. M.; Tang, S.; Bao, C.; Tang, P.; Qiu, F.; Zhu, L.; Zhao, B. *ACS Macro Lett.* **2012**, *1*, 1061−1065.
(29) Jinnai, H.; Spontak, R. J.; Nishi, T. *Macromolecules* **2010**, *43*, 1675−1688.
(30) Tseng, W.-H.; Chen, C.-K.; Chiang, Y.-W.; Ho, R.-M.; Akasaka, S.; Hasegawa, H. *J. Am. Chem. Soc.* **2009**, *131*, 1356−1357.
(31) Wang, X.-B.; Lo, T.-Y.; Hsueh, H.-Y.; Ho, R.-M. *Macromolecules* **2013**, *46*, 2997−3004.
(32) Lo, T.-Y.; Ho, R.-M.; Georgopanos, P.; Avgeropoulos, A.; Hashimoto, T. *ACS Macro Lett.* **2013**, *2*, 190−194.
(33) Mareau, V. H.; Akasaka, S.; Osaka, T.; Hasegawa, H. *Macromolecules* **2007**, *40*, 9032−9039.
(34) Chen, C.-K.; Hsueh, H.-Y.; Chiang, Y.-W.; Ho, R.-M.; Akasaka, S.; Hasegawa, H. *Macromolecules* **2010**, *43*, 8637−8644.
(35) Trent, J. S.; Scheinbeim, J. I.; Couchman, P. R. *Macromolecules* **1983**, *16*, 589−598.
(36) Assuming the P*t*BA and PS brushes have the same densities as the bulk samples (i.e., 1.008 g/cm^3 for P*t*BA and 1.052 g/cm^3 for PS), the volume fraction of PS in the mixed brushes is 37%.
(37) Feng, C. L.; Vancso, G. J.; Schonherr, H. *Langmuir* **2005**, *21*, 2356−2363.